Nonlinear spatiotemporal integration by electrical and chemical synapses in the retina
Sidney P. Kuo, Gregory W. Schwartz, Fred Rieke
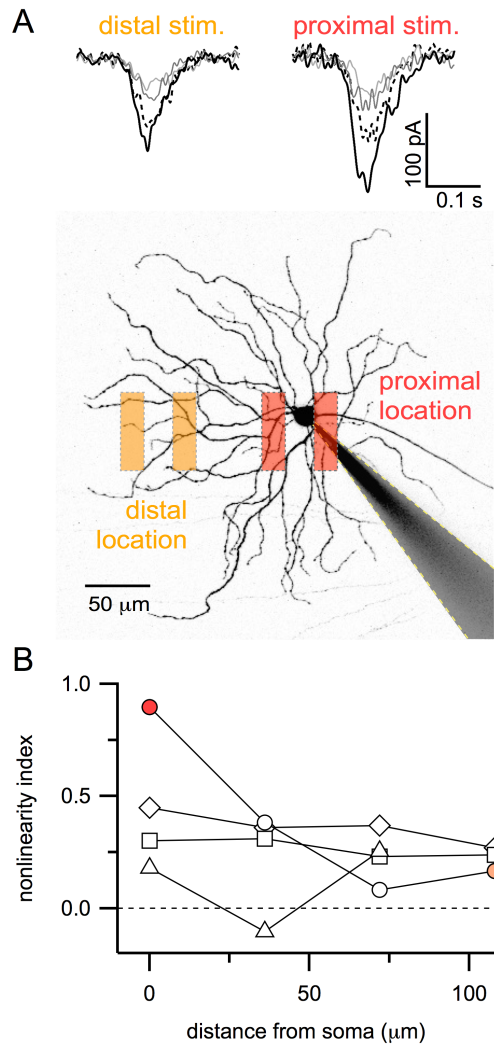
Supplemental Data

Figure S1, Related to Figure 1. Evidence that postsynaptic mechanisms do not contribute to excitatory current nonlinearities measured in voltage-clamp.

(A) Top panels, example mean responses (15 trials each) to stimulus locations distal (left, orange) or proximal (right, red) to somatic recording site. Dashed black line is sum of single bar responses (single bar responses in gray). Solid black line is actual response to

paired bar presentation. Bottom panel shows approximate stimulus locations overlaid over fluorescent dye-filled ON-S cell image acquired post-recording. Dashed yellow line and grayed area indicate boundaries of recording pipette.

(B) Summary of nonlinearity indices versus stimulus location (n=4 cells; different symbols correspond to different cells). Voltage-clamp errors should increase with distance from the somatic recording pipette (Williams and Mitchell, 2008). Thus, there should be a positive relationship between stimulus location and nonlinearity index if space clamp errors allow postsynaptic mechanisms to contribute to nonlinear paired bar responses. However, the example cell shown in (A) and in colored symbols in (B) showed the opposite relationship between stimulus location and nonlinear paired bar interactions; overall there was no difference between proximal and distal stimuli (stimuli centered over soma NLI = 0.45 ± 0.16; for stimuli centered 72 μm from soma, NLI = 0.23 ± 0.06; p = 0.35; paired t-test; n = 4 cells, mean ± SEM). In these experiments stimulus contrast was held constant within each cell and short bars (60 μm in length, 18 μm width) were used to uniformly probe the bipolar population presynaptic to the recorded RGC. Inter-bar spacing was 22 μm. Recordings were from large ON-S RGCs (dendritic diameter = 267 ± 18 μm, mean ± SEM) (Bleckert et al., 2014), in which potential voltage-clamp errors should be most problematic.
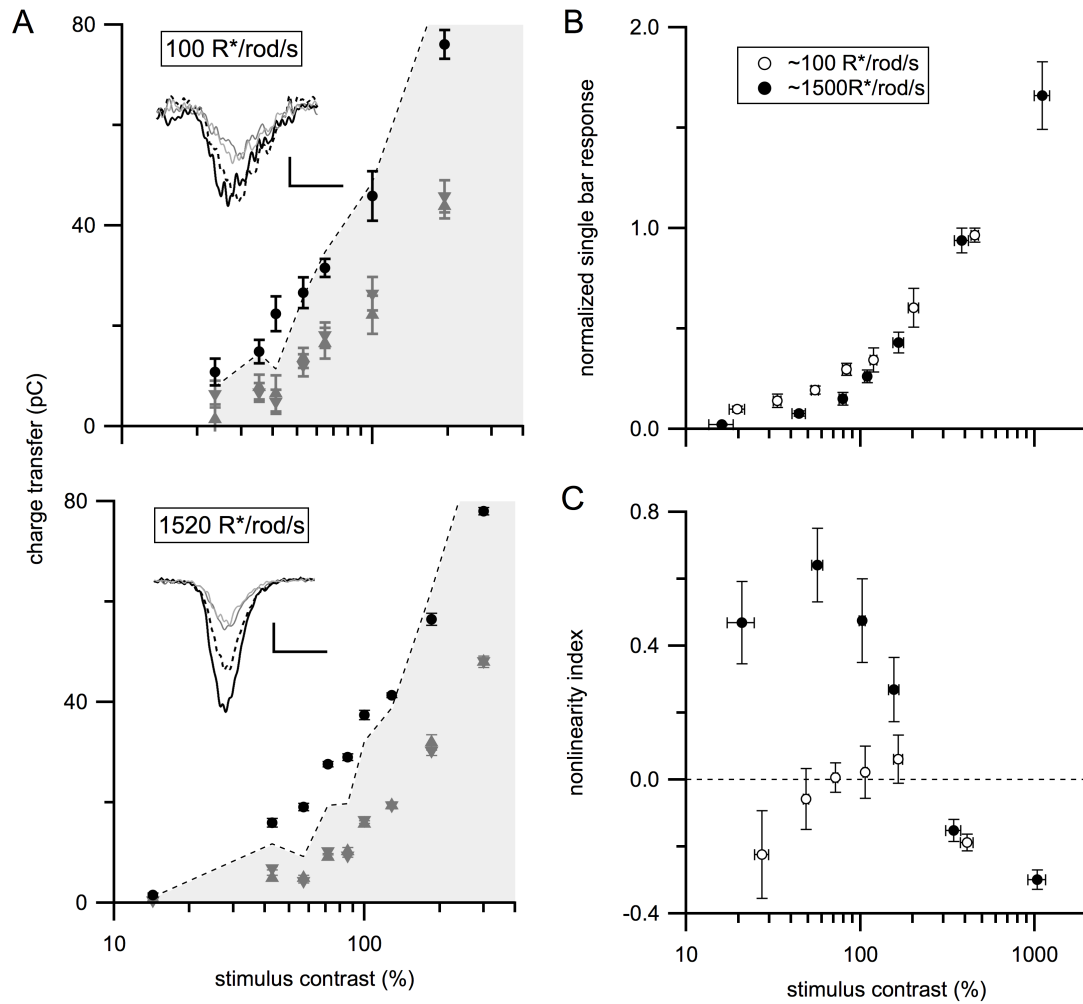
Figure S2, Related to Figure 2. Nonlinear integration depends on background light level
(A) Single (gray triangles) and paired bar responses (filled black circles) across contrasts at ~100 R*/rod/s (top) and ~1500 R*/rod/s (bottom) in the same ON-S RGC. Dotted black line and grayed area shows linear sum of single bar responses. Insets show example currents at different backgrounds (53% and 71% contrast, top and bottom, respectively). Vertical and horizontal scale bars in insets represent 100 pA and 0.1 s, respectively. (B) Summary contrast-response relationships across cells for single bar stimuli (~100 R*/rod/s, n = 6 cells, gray open circles; ~1500R*/rod/s, n = 5 cells, filled black circles). (C) Summary nonlinear indices across contrasts at each background light level. Same color and symbol scheme as (B).
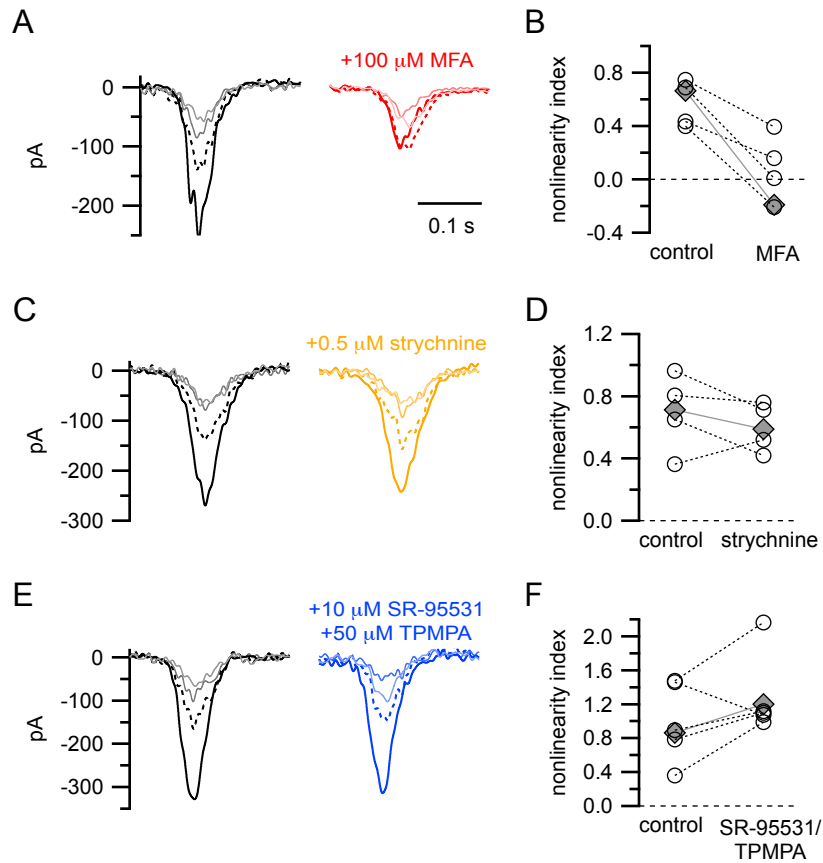
Figure S3, related to Figure 3. Nonlinear integration is reduced by pharmacological block of gap junctions, but not antagonists of inhibitory synaptic transmission.

(A) Example single and paired bar responses in ON-S RGC prior to (control, black) and during bath application of 100 μM MFA (red). Light, thin lines indicate single bar responses, dashed lines indicate sum of single bar responses and dark, thicker lines indicate paired bar responses.

(B) Summary data for experiments using 100 μM MFA. Symbols connected with lines indicate data from different cells. Gray diamonds indicate data from example cell in (A). Nonlinearity indices were significantly reduced in the presence of MFA (p <0.007, paired t-test; n=5 cells). In all cells, stimulus contrast in the presence of MFA was increased in order to elicit similar amplitude single bar responses as in control (contrast in MFA = 453 ± 136% of control contrast). We note these results must be interpreted cautiously (see '*Caveats of meclofenamic acid*' in Supplemental Experimental Procedures, below).

(C-D) Same as for (A-B), but for bath application of 0.5 µM strychnine, which did not affect nonlinear integration (control NLI = 0.70 ± 0.10, strychnine = 0.60 ± 0.06; p = 0.25, paired t-test; n=5 cells). Because strychnine application enhanced sensitivity to single bar stimuli, we lowered stimulus contrast slightly during strychnine incubation so as to match single bar responses in drug to control responses (contrast in strychnine = 61 ± 10% of control contrast).

(E-F) Same as for (A-B), but for co-application of 10 µM SR-95531 and 50 µM TPMPA. Unlike the case for MFA or strychnine, SR-95531+TPMPA did not systematically alter retinal sensitivity so we did not need to adjust stimulus contrast between control and drug conditions in most cases. Similar to strychnine, nonlinear integration was not significantly affected by co-application of SR-95531 and TPMPA (control NLI = 0.97 ± 0.17, drugs = 1.28 ± 0.18; p=0.11, paired t-test; n=6 cells).
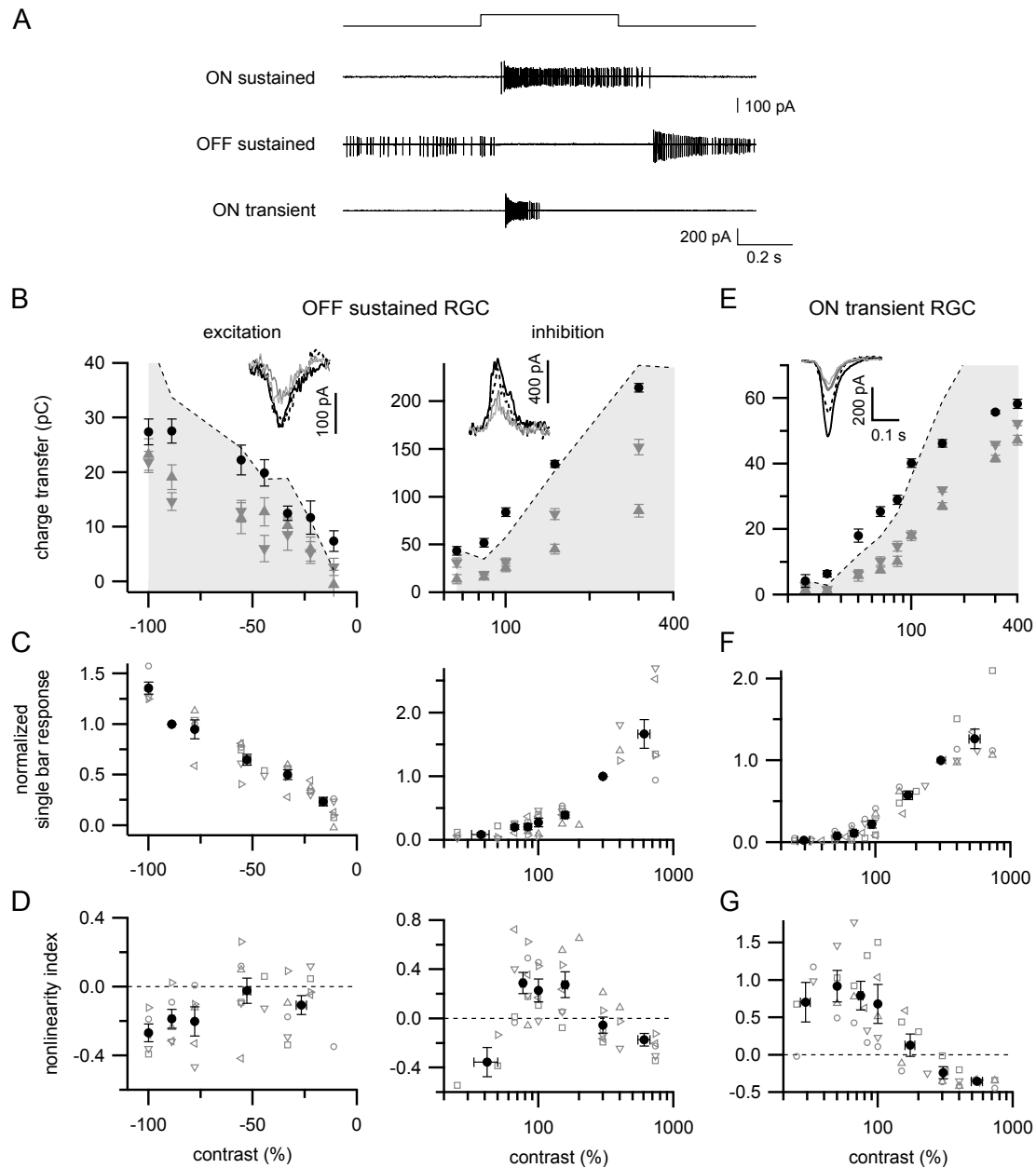
Figure S4, related to Figure 2. Nonlinear paired bar interactions in additional RGC types.
(A) Example cell-attached recordings of spike responses to ~30R*/rod/s light steps (300
μm spot centered on soma) from nominal darkness in anatomically and functionally
distinct RGC types.
(B) Example excitatory (left) and inhibitory (right) postsynaptic currents in an OFF-S
RGC to negative or contrast bar stimuli. Gray symbols show single bar responses, black
circles show paired bar responses. Dashed lines indicate linear sum of single bar

responses. Insets show example cell responses at -22% contrast (left) or +83% contrast (right).

(C-D) Summary data from OFF-S RGCs for single bar responses (C) and nonlinearity index (D) for excitatory and inhibitory currents (n=6 cells for each type of recording). Gray symbols indicate data from individual cells, black circles with error bars show mean±SEM.

(E) Positive contrast bar stimulus-evoked excitatory currents in an example ON-T RGC. Same color and symbol scheme as (B).

(F-G) Summary data from ON-T RGCs (n=5 cells). Same symbol and color scheme as (C-D).

For recordings in (B-G), stimuli were restricted to a 360 µm-diameter circle centered on the RGC soma and bar width=18 µm, inter-bar spacing=22 µm.
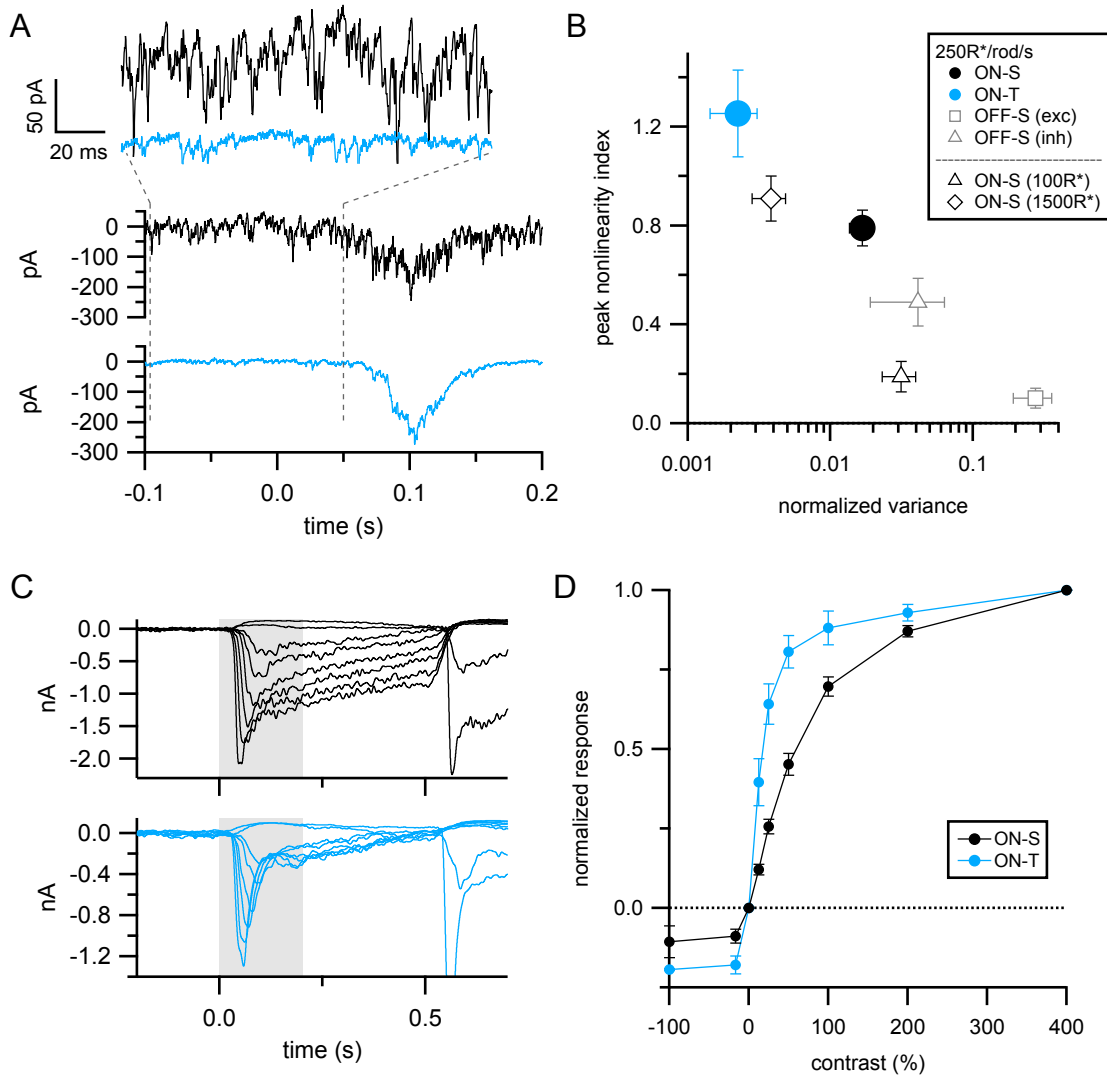
Figure S5, related to Figure 2. Distinct excitatory synaptic input to ON-S versus ON-T RGCs.

(A) Example excitatory synaptic currents in an ON-S (black) or ON-T (blue) RGC. Bar stimulus (single 18 µm-wide bar, 200% contrast, 33ms flash) was presented at time=0 s. Currents from the time period prior to the bar-evoked response (indicated by gray dashed lines) are shown above at expanded time and current scale.

(B) Population data for peak nonlinearity index plotted against normalized holding current variance (holding current variance divided by for different RGC types and, for ON-S RGCs, different background light levels. Normalized variance ($\sigma^2_{normalized}$) was calculated as:

$$\sigma^2_{normalized} = \frac{\sigma^2}{P^2}$$

where σ^2 is the holding current variance and p is the peak response at +200% (ON-S, ON-T, OFF-S inhibition) or -50% contrast (OFF-S RGC excitation). In those recordings in which we did not present +200 (or -50%) contrast bar stimuli, we fit the single bar contrast-response relationships with a Hill function to estimate the response at +200 (or -50%) contrast. Note higher peak nonlinearity and lower normalized holding current variance in ON-T versus ON-S RGCs at 250R*/rod/s.

(C) Excitatory currents recorded in example ON-S (black) or ON-T (blue) RGCs in response to 300 μm diameter spot stimuli (0.5 s step, starting at time=0 s) presented at -100 to +400% contrast. Gray boxes show region of response (0-0.2 s following step onset) over which currents were integrated to quantify responses.

(D) Summary data from ON-S (n=8 cells) and ON-T (n=3 cells) RGCs. Responses in each cell were normalized to the response at +400% contrast. Note steeper contrast-response relationship in ON-T compared to ON-S RGCs.

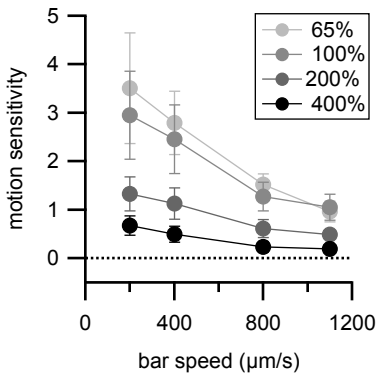
Figure S6, Related to Figure 7. Enhanced sensitivity to apparent motion at different bar movement speeds

Motion sensitivity, calculated as in Figure 7 from responses to sequential or randomized bar stimulus presentations, versus apparent motion speed. Circles with error bars show mean ± SEM for n=6 cells. Gray levels indicate stimulus contrast of the bar stimuli, as indicated in the legend.

Supplemental Experimental Procedures

Tissue preparation

Experiments were conducted in tissue obtained from 5-15 week old wild-type or

cx36-/- (Deans et al., 2002), *Grm6-tdTomato* (Morgan et al., 2011), *Gus8.4-EGFP*

(Huang et al., 1999), or *Gjd2-EGFP* (The Gene Expression Nervous System Atlas

(GENSAT) Project, NINDS Contract #N01NS02331 and HHSN271200723701C to the

Rockefeller University (New York, NY)) transgenic mice. All transgenic mice were

backcrossed into the same genetic background as wild-type (C57BL/6J; Jackson Labs).

Mice were dark-adapted overnight prior to use and all tissue preparation procedures were

conducted using infrared light (>950 nm) to preserve visual sensitivity. Retinal flat

mounts used for RGC and AII amacrine recordings were prepared as previously

described (Schwartz et al., 2012). Briefly, the cornea, lens and vitreous were dissected

from both eyes in warmed (~32°C), oxygenated (95% O_2, 5% CO_2), bicarbonate-buffered

Ames solution. Eye-cups were then stored in the same solution in a light-tight container

and allowed to recover at 32°C for >45 minutes before use because we found this

improved stability of visual responses. After this resting period, a piece of retina was

detached from the sclera and adhered with the RGC layer facing up onto a poly-D-lysine

coated glass coverslip (Corning) in a recording chamber. For bipolar recordings, a

vibratome (Leica) was used to prepare vertical slices (200 μm thick) from retinas that

were initially isolated following the same procedure as for flat mounts. As in previous

work (Grimes et al., 2014b), isolated retina was embedded in low melting point agarose

(Sigma) and sectioned in an orientation perpendicular to the flat-mount plane in ~22°C,

oxygenated (100% O_2) HEPES-buffered Ames solution. Slices were either stored until

use at 32°C in bicarbonate-buffered, oxygenated Ames solution or immediately

transferred to a recording chamber. Retinal slices were prepared exclusively from ventral

retina. Flat mount recordings were obtained from both ventral and dorsal retina; we did

not observe obvious differences across retinal location so results were pooled. Recordings

in flat mounts were conducted within ~7 hours of initial tissue dissection. Slice

recordings were obtained <~4 hours after slicing.

Electrophysiology

During recordings, retinal tissue was continuously perfused (~8 mL/min) with

oxygenated, bicarbonate-buffered Ames solution maintained at 30-34°C. Retinal neurons

were visualized and targeted for patch-clamp recordings using infrared (>950 nm)

differential interference contrast microscopy. Whole-cell voltage-clamp recordings were

obtained using patch pipettes (RGC: 2.5-3.5 MΩ; AII amacrine: 8-10 MΩ; bipolar: 10-12

MΩ open tip resistances) filled with an internal solution composed of (in mM): 105 Cs-

methanesulfonate, 10 Tetraethylammonium-Cl, 20 HEPES, 10 EGTA, 2 QX-314, 5 Mg-

ATP, 0.5 Tris-GTP; ~280 mOsm; pH adjusted to 7.3 using CsOH. For all AII amacrine

recordings and in a subset of RGC recordings, 100-200 μM Alexa Fluor 594-hydrazide or

Alexa Fluor 750 hydrazide (Molecular Probes) was included in this solution. For all

bipolar recordings, 50-100 μM GTP-γ-S and 100-200 μM Alexa Fluor 594 were added to

the Cs-based internal solution and 10 μM NBQX (Tocris) was added to the bath

perfusion solution. Whole-cell current-clamp recordings from AII amacrines used an

internal solution composed of (in mM): 123 K-aspartate, 10 KCl, 10 HEPES, 1 $MgCl_2$, 1

$CaCl_2$, 2 EGTA, 4 Mg-ATP, 0.5 Tris-GTP and 0.1-0.2 Alexa Fluor 594-hydrazide or

Alexa Fluor 750-hydrazide (~280 mOsm; pH ~7.2 with KOH). RGC spiking activity was measured using loose-cell attached recordings with pipettes (8-10 MΩ) filled with Ames solution. Voltage-clamp recordings were conducted with cells held at -68.5 mV, near the reversal potential for inhibitory conductances, to isolate excitatory currents. In all RGC recordings, series resistance (<15 MΩ) was compensated by 70% using the amplifier circuitry (Multiclamp 700B; Molecular Devices). Series resistance was left uncompensated in voltage-clamp recordings from AII amacrines and cone bipolar cells. No holding current was applied during current-clamp recordings from AII amacrines (resting membrane potential = -48 ± 2 mV; n = 5 cells). Reported membrane potential values are corrected for measured liquid junction potentials of -8.5 mV and -10.8 mV for the Cs-based and K-based solutions, respectively. Electrical signals were acquired at 10 kHz and low-pass filtered at 3 kHz. Current traces presented in the figures were additionally low-pass filtered at 100 Hz for display purposes. For bath application of drugs, pharmacological reagents were diluted to final working concentrations in Ames solution from concentrated aqueous stock solutions that were prepared then at stored at -20°C (NBQX (Tocris), strychnine, TPMPA, SR-95531 (Tocris)), or, in the case of MFA (Sigma or Alfa Aesar), from stock solution that was freshly prepared each day. Unless otherwise noted, chemicals were obtained from Sigma.

Cell identification

ON-S and OFF-S RGCs were identified by their large soma size (~15-20 μm diameter) and characteristic spiking responses to step light increments (Murphy and Rieke, 2006; van Wyk et al., 2009; see Figure S4). In some cases, dendritic morphology

of fluorescent dye-filled cells was examined following recordings and confirmed to be

consistent with ON-S (Bleckert et al., 2014) or OFF-S (van Wyk et al., 2009) RGCs. ON-

T RGCs were identified by their transient spike responses to step stimuli (Figure S4). In

related work, we have found that the dendrites of these RGCs tightly co-stratify with the

axons of type 5 bipolar cells and receive a large fraction of their excitatory synaptic input

from a specific type 5 bipolar cell subtype (S. Kuo, H. Okawa, F. Rieke, R. Wong,

unpublished). AII amacrines were targeted in the flat mount preparation by identifying

cells with small somas (<10 μm diameter) located within the region of the inner nuclear

layer most proximal to the ganglion cell layer. AII amacrines also were readily

distinguished by several electrophysiological characteristics, including robust

spontaneous excitatory synaptic input (Grimes et al., 2014a), evidence of voltage-gated

Na^+ currents (Tian et al., 2010), and gap junction-mediated excitatory inputs that were

insensitive to holding potential. Additionally, we used fluorescence microscopy to

confirm that the dendrites of each recorded cell exhibited the narrow-field arborization

and distinct stratification pattern characteristic of AII amacrine cells (Tsukamoto et al.,

2001). ON cone bipolar cells in retinal slices from wild-type mice were targeted based on

soma shape and location within the inner nuclear layer. In some cases, ON cone bipolar

subtype-specific expression of fluorescent proteins (tdTomato or EGFP) in transgenic

mice was used to target recordings using two-photon laser scanning excitation (960 nm).

In these instances, we minimized light exposure from the two-photon laser (Euler et al.,

2009) by restricting scan regions (85 x 85 μm) to the inner retina, away from

photoreceptors, and by keeping laser exposure brief (<30 seconds per scan region; < 2

mW post-objective laser power). Following all bipolar recordings, dye-filled cells were

imaged and classified into subtypes according to axon terminal morphology and stratification level within the inner plexiform layer (Wassle et al., 2009). Fluorescent protein expression was also used for bipolar classification when applicable.

Visual stimulation

For RGC and AII amacrine recordings, spatially patterned visual stimuli were delivered from an OLED monitor (eMagin; 800 x 600 pixels, 1.2 or 1.8 µm per pixel at the preparation; 60 Hz frame rate). For bipolar recordings, light stimuli consisted of a spatially uniform circular spot (520 µm diameter) delivered from a short-wavelength LED (peak spectral output 405 nm; Hosfelt). In both cases, stimuli were projected through the microscope condenser and focused on the photoreceptor layer. Bar stimuli were 18 µm wide and restricted to a region centered on the soma of the recorded cell (360 x 360 µm square in Figure 7 and Supp. Figure S6; otherwise 360 µm-diameter circle). With the exception of Figure 6C-D, Figure 7 and Supp. Figure S6, bars were presented for two stimulus monitor frames (33 ms). Except in supplementary Figure S2, RGC and AII amacrine recordings were performed with a background light intensity of ~250 photoisomerizations per rod per second (R*/rod/s). Recordings were obtained ≥ 10 minutes after applying background illumination. Background illumination was applied using the entire extent of the stimulus monitor, except in the case of RGC recordings from *cx36-/-* retinas, where the drastically reduced retinal sensitivity and limited dynamic range of the OLED monitor necessitated presenting the background light from a separate green LED (peak spectral output 470 nm; 560 µm diameter spot). Bipolar responses were measured on a background of ~600 R*/rod/s except for recordings from *cx36-/-* tissue,

when responses were obtained from nominal darkness due to reduced sensitivity of bipolar cells in *cx36-/-* retinas. In these recordings, stimuli consisted of brief full-field flashes (10 ms duration; ~100 R*/rod/flash in wild type; ~600R*/rod/flash in *cx36-/-*).

Analysis

Responses to bar stimuli were quantified by integrating measured currents or voltages over a post-stimulus window defined by the times when the rise and decaying phase of responses reached 5% of the peak response amplitude, or by integrating over a fixed 175 ms-long window that began 25 ms after stimulus onset. The latter approach was used in those experiments where responses were compared across contrasts (stimulus-response relationships in Figures 3 and 4, supplementary Figure S2) so that responses were integrated over a window with fixed duration. However, these approaches produced similar results.

For the apparent motion and randomized bar stimuli (Figure 8), excitatory input was quantified by integrating currents over the duration of the stimulus presentations. Spiking activity in those experiments was quantified as the mean spike rate over the duration of the stimulus presentation. Apparent motion sensitivity (*MS*) was quantified similar to the NLI used to quantify paired bar effects:

$$MS = \frac{R_{motion} - R_{random}}{R_{random}}$$

where R_{motion} and R_{random} were the current or spike responses to the apparent motion or randomized bar stimuli, respectively.

Responses in bipolar cells were quantified by measuring peak amplitudes of responses. 'Peak' and 'steady-state' responses reported in Figure 5C were the largest

15

response within the first 15 sec after establishing whole-cell configuration and the mean response to 10 consecutive stimulus presentations during the plateau phase of the recording, respectively. We restricted our analysis of bipolar responses to those cells with responses during the first 15 seconds of whole-cell recording greater than the mean + 2 SD of the steady-state response. We used this criteria to ensure we captured at least some of the intrinisic response of the recorded bipolar cell in our measurement. Presumably, in those recordings that did not exhibit a clear intrinsic component to their response, we did not start data acquisition quickly enough and/or some cones providing direct input to the recorded bipolar were damaged in the slicing procedure. However, every ON cone bipolar tested exhibited a GTP-γ-S-insensitive response consistent with those shown in Figure 5. Reported values are mean ± SEM. Except for the single trial examples in Figures 1C-D and 4B, all current and voltage traces are mean responses to 8-12 individual stimulus presentations. Spike PSTHs and mean spike rates (Figure 7) are from 25 trials per stimulus condition.

Caveats of meclofenamic acid

We used bath application of meclofenamic acid (MFA) (Supplementary Figure S3) to corroborate our results from *cx36-/-* mice that gap junctions are required for nonlinear paired bar interactions. However, these experiments were made challenging by drastic effects of MFA on the sensitivity and health of isolated retinal tissue. In every ON alpha RGC voltage-clamp recording we attempted (n = 5 cells), bath application of 100 μM MFA caused a sudden and precipitous (>1nA) increase in holding current after a variable amount of time following the start of drug application (mean ± SEM: 21.2 ± 4.2

min; range = 10 – 31 minutes; n=5 cells). Over the same time-course, the light sensitivity of the retina declined and the structure of the retina became visibly altered such that by the time the recording was lost, the surface of the ganglion cell layer appeared uniformly pockmarked and the inner plexiform layer looked grainy. In cases where the recording lasted for ≥ ~20min, sensitivity of the tissue typically declined to the point where it was no longer possible to evoke light responses using bar stimuli at up to ~800% contrast. Further, we were not able to successfully establish GΩ seals from RGCs in tissue that had previously been exposed to 100 µM MFA. Application of lower concentrations of MFA improved the duration over which RGC recordings could be maintained, but still usually resulted in loss of the recording and associated changes in tissue appearance within an hour following the start of drug application (at 75 µM MFA, recordings lasted 43.5 ± 6.9 minutes from start of drug application for n= 6 cells; for five cells at 50 µM, two cells lasted > 45 min while the remaining three died at 32 ± 7.8 min). For these reasons, we conclude that, at least in our hands, bath application of MFA kills isolated retinal tissue over a similar time course and at a similar concentration for which the drug has previously been shown to block gap junction-mediated signaling (Pan et al., 2007; Veruki and Hartveit, 2009). The data shown in Supplementary Figure S3A-B shows responses to single and paired bar stimuli prior to the start of MFA application (control), or in the presence of 100 µM MFA within a time window just prior to loss of the recording.

Modeling

As in previous work (Schwartz et al., 2012), model bipolar locations were defined according to a jittered hexagonal grid with 16 µm grid spacing plus Gaussian noise (SD =

2 μm) and model input consisted of contrast values at each pixel of a two-dimensional stimulus, *S(x,y)*. Unlike the previous model, stimulus-independent variability in initial bipolar states across the population was simulated by initializing each bipolar cell with an effective contrast, c_{noise}, which was drawn randomly from a Gaussian distribution. Because we introduced variability prior to gap-junction mediated spread of signals, our implementation approximated the effects of dynamic fluctuations in bipolar membrane potential. However, introducing variability after gap-junction mediated signal spread spread, which simulates static voltage differences between bipolar cells (e.g. steady differences in V_{rest}), produced similar results (not shown). Stimulus-evoked dendritic input to each model bipolar was calculated by multiplying the dendritic receptive field of each bipolar, *F$_{dendrite}$(x,y)*, by the stimulus, *S(x,y)*, and summing across each point:

$$c_{dendrite} = \sum_{x,y} S(x,y)\, F_{dendrite}(x,y)$$

F$_{dendrite}$(x,y) was defined by a two-dimensional circular Gaussian profile with standard deviation, σ (see Figure 5D). Thus, the response (in units of contrast), c_b, for a given model bipolar prior to spread through gap junctions was defined by:

$$c_{b(i)} = c_{dendrite(i)} + c_{noise(i)}$$

Electrical coupling across the bipolar network was simulated by distributing a fraction of c_b to neighboring bipolar cells by taking into consideration the distance and effective driving force between every pair of bipolar cells:

$$c_{gj(i)} = \sum_{j=1}^{n} g\big(c_{b(i)} - c_{b(j)}\big) e^{\left(\frac{-d(i,j)}{\lambda}\right)}$$

where *n* is the total number of bipolars in the population, *d(i,j)* is Euclidean distance between center locations of bipolars *i* and *j*, λ is a space constant for signal spread via gap

18

junctions, and g is the maximal fraction of c_b signal transmitted through gap junctions. Gap junction-derived signals were summed with the dendritic input and bipolar noise to give the total response of a given bipolar:

$$c_{total(i)} = c_{b(i)} + c_{gj(i)}$$

Finally, synaptic output from each bipolar was calculated by using the total bipolar response, c_{total}, as the input to a nonlinear function defined by the Hill equation:

$$r_i = \frac{1}{1 + (\frac{c_{half}}{c_{total(i)}})^h}$$

where c_{half} and h are parameters that determine the offset along the contrast axis and steepness of the contrast-response function, respectively. Output from each bipolar was then weighted and summed to produce the total model excitatory input to an RGC, T:

$$T = \sum_{i=1}^{n} W_i r_i$$

Bipolar weights, W, were defined according to a circular Gaussian profile with a one SD width of 150 µm. We considered it appropriate to model the RGC receptive field using a Gaussian profile, rather than with a model that takes into account detailed dendritic structure (Schwartz et al., 2012), because our stimuli extended over most of the dendritic span of an ON-S RGC dendrite, which should reduce potential effects of dendritic morphology.

Supplemental References

Euler, T., Hausselt, S. E., Margolis, D. J., Breuninger, T., Castell, X., Detwiler, P. B., and Denk, W. (2009). Eyecup scope--optical recordings of light stimulus-evoked fluorescence signals in the retina. Pflugers Arch *457*, 1393-1414.

van Wyk, M., Wassle, H., and Taylor, W. R. (2009). Receptive field properties of ON- and OFF-ganglion cells in the mouse retina. Vis Neurosci *26*, 297-308.